AIAA JOURNAL
Vol. 49, No. 12, December 2011

Vortex Shedding and its Nonlinear Acoustic Effect Occurring at a Slit

Xiwen Dai,* Xiaodong Jing,† and Xiaofeng Sun*
Beijing University of Aeronautics and Astronautics, 100191 Beijing, People's Republic of China

DOI: 10.2514/1.J051086

This paper presents a theoretical study of the nonlinear acoustic properties of a slit in a thin plate subjected to high-intensity sound excitation. In the present model, the conventional discrete vortex method is employed to simulate the near-field two-dimensional unsteady flow in order to capture the mechanism of the sound–vortex interaction, which is in combination with a spanwise-averaged three-dimensional Green's function method used to connect the near-field flow quantities with the far-field sound pressure. This model is compared with an existing particle image velocimetry flow visualization and a direct numerical simulation model, showing good qualitative agreement. It is revealed that the oscillatory slit flow is dominated by a pair of spiral-like counter-rotating vortices moving away from the slit and eventually colliding into each other. Because of the vortical flow effect, increases in the sound pressure level result in significant increases in acoustic resistance and modest decreases in acoustic reactance. For the parametric range in this study, increases in the aspect ratio of the slit result in slight increases in acoustic resistance but unnegligible reductions in acoustic reactance. However, the influence of the aspect ratio on acoustic impedance tends to be less important when the sound pressure level exceeds a certain high value.

Nomenclature

AR	=	aspect ratio of slit
b	=	length of slit
C	=	inertia coefficient
c	=	sound speed
C_D	=	discharge coefficient
D	=	depth of back cavity
d	=	length of feeding sheet of nascent vortex
f	=	frequency
k	=	wave number, ω/c
$\boldsymbol{l}$	=	vector length along integration path ACB
N	=	number of discrete vortices
P	=	amplitude of applied sound pressure
p_i	=	incident sound pressure
p_r	=	reflected sound pressure
Q	=	volume flux through slit (strength of point source in ζ plane)
r	=	normalized acoustic resistance
r_c	=	cutoff radius of vortex blob
s	=	half width of slit
SPL	=	applied sound pressure level
T	=	time period
t	=	time
t_0	=	initial time
$\mathbf{u}_Q$	=	velocity due to slit flow
$\mathbf{u}_\Gamma$	=	velocity due to discrete vortices
$u^{\pm}$	=	acoustic particle velocity on right and left sides of slit plate
v_{av}	=	average velocity through slit
$v_{\text{av}}(n)$	=	amplitude of nth harmonic of v_{av}
v_{VC}	=	velocity at vena contracta
W	=	complex potential
w	=	complex velocity
W_Q	=	complex potential due to slit flow
W_Γ	=	complex potential due to discrete vortices and their images
x	=	normalized acoustic reactance
(x_1, x_2, x_3)	=	Cartesian coordinates in physical plane
z	=	complex coordinate in physical plane
Z_{cavity}	=	normalized acoustic impedance of cavity
Z_{res}	=	normalized acoustic impedance of Helmholtz resonator
Z_{slit}	=	normalized acoustic impedance of slit
z_e	=	complex coordinate of slit edge in the physical plane
z_n	=	complex coordinate of nth discrete vortex in the physical plane
Γ	=	circulation
Γ_n	=	circulation of nth discrete vortex
Γ_t	=	total circulation of shed vortex
Γ_1	=	circulation of nascent vortex
Δt	=	time interval
ζ	=	complex coordinate in the conformal mapping plane
ζ_n	=	complex coordinate of nth point vortex in the conformal mapping plane
κ	=	smooth parameter
(ξ_1, ξ_2)	=	Cartesian coordinates in the conformal mapping plane
ρ	=	air density
σ	=	open area ratio of perforated plate
$\phi(1)$	=	phase of the first harmonic of v_{av}
Φ_Q	=	quasi-three-dimensional potential function
ω	=	angular frequency

Received 20 November 2010; revision received 1 June 2011; accepted for publication 11 June 2011.

*Fluid and Acoustic Engineering Laboratory, School of Jet Propulsion.
†Fluid and Acoustic Engineering Laboratory, School of Jet Propulsion; jingxd@buaa.edu.cn (Corresponding Author).

I. Introduction

PERFORATED liners in the form of cavity-backed orifices are used successfully to reduce the amount of noise emitted from commercial aircraft engines. Modern commercial aircraft highly depend on the liner technology to meet the increasingly stringent noise regulations. With rare exception, the orifices in a perforated liner are in a circular shape. So, it is of interest to study the acoustic properties of a slit or a rectangular orifice with a large aspect ratio and then make a comparison with the well-used circular orifice.

Indeed, the use of slit as an acoustic element has drawn the attention of researchers for many years [1–4]. However, most of the

investigations concentrated on the viscous dissipation of the acoustic energy at the slit [1–4]. When there is high-intensity sound and flow present, as typically occurs in an aeroengine nacelle, the acoustic energy dissipation at an orifice is dominated by the mechanism of the sound–vortex interaction. Howe [5] described the process as the flow separation and vortex shedding at the sharp edge leading to the conversion of the acoustic energy into unsteady vortical motion. This rotational energy cannot be reverted back into acoustic energy. It is eventually dissipated into heat by molecular viscosity.

There have been numerous studies regarding the sound–vortex interaction at a circular orifice. However, this mechanism has not been thoroughly investigated for slits. When there is either mean bias flow or grazing flow present, linear assumption has been employed to model the sound–vortex interaction, and thus the acoustic properties of slits in a screen [6,7]. However, when subjected to high-intensity sound, a slit shows strong nonlinear acoustic properties, just as a circular orifice [8–12]. Recently, Tam et al. [13,14] used direct numerical simulation (DNS) to capture the details of the unsteady flow excited by high-intensity sound impinged on a slit, from which they obtained the gross effect of the acoustic impedance of the slit. In their simulation, both the viscous and the sound–vortex interaction mechanisms are simultaneously taken into account.

In the present paper, a slit in an infinitely large thin plate subjected to high-intensity sound is considered, with emphasis on the sound–vortex interaction mechanism. For high Reynolds number cases, the vorticity is confined to a compact region in the flowfield around the slit. As a result, the viscous effect can be neglected everywhere except for the slit edges, where the Kutta condition is applied to account for the generation of the vortices. To capture the flow details of the vortex shedding and evolution around the slit, a discrete vortex model (DVM) is set up on the assumption that the slit is infinitely long. Then, the near-field two-dimensional (2-D) flow simulation results are substituted into a spanwise-averaged three-dimensional (3-D) Green's function integral formula to compute the acoustic resistance and the reactance of the slit. Thus, in contrast to the previous axisymmetrical DVM for the acoustic nonlinearity of a circular orifice [15], the present model combines the 2-D DVM and the 3-D Green's function to develop a quasi-3-D numerical strategy to deal with the problem of the acoustic nonlinearity occurring at a slit. The details of the present model are given in the next section. In Sec. III, we first compare the present results with those of the DNS obtained by Tam et al. [13], and then we provide an analysis and discussion based on the present computation. Finally, the paper finishes with conclusions in Sec. IV.

II. Setting up of the Model

In Fig. 1, a slit in an infinitely large thin plate subjected to the excitation of a high-intensity sound wave is shown. The acoustic pressure drives the oscillatory flow through the slit, resulting in the unsteady vortex shedding at the slit edges. Thus, by the mechanism of dynamical exchange between the acoustic and vortical motions, the acoustic behavior of the slit is highly dependent on the amplitude of the incident sound pressure.

If the sound wavelength is much larger than the size of the slit, the unsteady flow around the slit can be approximately treated as incompressible. For this condition, the incident sound wave is considered as the fluctuating pressure uniformly distributed in the far field:

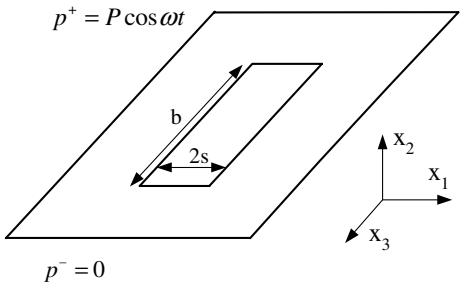

Fig. 1 Slit in a thin plate subjected to the high-intensity sound wave.

$$p_i = \begin{cases} P\cos\omega t & (x_2 > 0, x_1^2 + x_2^2 + x_3^2 \to \infty) \\ 0 & (x_2 < 0, x_1^2 + x_2^2 + x_3^2 \to \infty) \end{cases} \tag{1}$$

where a sinusoidal time dependency has been assumed. When the Reynolds number is high, the viscous effect can be neglected everywhere except for the slit edges where vortex shedding takes place. Therefore, we can suitably employ the DVM to describe the sound–vortex interaction phenomenon, in which the vortex shedding and the evolution of the shear layers near the slit are depicted by an array of discrete vortices. It is also assumed that the slit has a large aspect ratio, such that the motion of the discrete vortices, mainly occurring in the vicinity of the slit, can be computed according to the Kelvin theorem. Furthermore, in order to compute the nonlinear acoustic impedance of the slit, a quasi-3-D potential model for the far-field fluctuating pressure is set up in collaboration with the near-field 2-D DVM.

A. Two-Dimensional Discrete Vortex Model for the Near-Field Unsteady Flow

The variables are nondimensionalized as

$$\bar{t} = \omega t, \qquad \bar{L} = L/s, \qquad \bar{V} = V/\omega s, \qquad \bar{\Phi} = \Phi/\omega s^2$$
$$\bar{p} = p/\rho\omega^2 s^2, \qquad \bar{\Gamma} = \Gamma/\omega s^2, \qquad \bar{Q} = Q/\omega s^2$$

where L, V, Φ, and p generally represent the distance, velocity, velocity potential, and pressure, respectively. The bars are omitted from the nondimensional variables for convenience hereafter in this section.

The 2-D incompressible assumption allows the near-field flow to be solved by means of the complex variable theory. The Schwartz–Christoffel transformation is written as follows:

$$z = \frac{1}{2}\left(\zeta + \frac{1}{\zeta}\right) \tag{2}$$

and the conformal mapping from the z plane to the ζ plane is as shown in Fig. 2. In the ζ plane, the complex potential W has two components: 1) W_Γ of the discrete vortices and their images, and 2) W_Q of the fluctuating flow through the slit that is conveniently given by a point source at the origin; that is,

$$W = W_Q + W_\Gamma = \frac{Q}{\pi}\ln\zeta + \sum_n \frac{\Gamma_n}{2\pi i}[\ln(\zeta - \zeta_n) - \ln(\zeta - \zeta_n^*)] \tag{3}$$

Note that the asterisk denotes the complex conjugate throughout this paper. The resulting complex velocity is given by the derivative of Eq. (3):

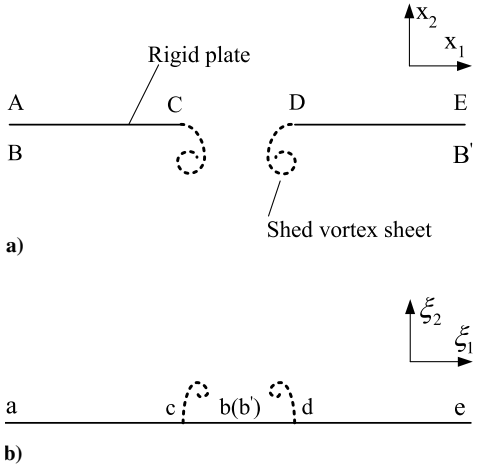

Fig. 2 Conformal mapping: a) physical domain and b) conformal transformation domain.

$$w^*(z) = \frac{\mathrm{d}W}{\mathrm{d}z} = \frac{\mathrm{d}W}{\mathrm{d}\zeta}\frac{\mathrm{d}\zeta}{\mathrm{d}z} \tag{4}$$

When the above equation is used to compute the convection velocity of each discrete vortex, special care must be taken such that the induced velocity due to the vortex itself is excluded. Then, for the nth point vortex,

$$w^*(z_n) = \lim_{z\to z_n}\frac{\mathrm{d}}{\mathrm{d}z}\left[W + \frac{\Gamma_n}{2\pi i}\ell_n(z - z_n)\right] = \left.\frac{\mathrm{d}\tilde{W}}{\mathrm{d}z}\right|_{z_n} + \frac{\Gamma_n\zeta''(z_n)}{4\pi i\zeta'(z_n)} \tag{5}$$

where $\tilde{W}(z)$ denotes the complex potential excluding the contribution of the nth discrete vortex. The second term on the right-hand side of Eq. (5) is the so-called Routh's correction. Substituting Eq. (3) into Eq. (5) yields

$$w^*(z_n) = \left(\frac{2\zeta_n^2}{\zeta_n^2 - 1}\right)\left[\frac{Q}{\pi\zeta_n} + \sum_{\substack{n'\\ n'\neq n}}\frac{\Gamma_{n'}}{2\pi i}\frac{1}{\zeta_n - \zeta_{n'}} - \sum_{n'}\frac{\Gamma_{n'}}{2\pi i}\frac{1}{\zeta_n - \zeta_{n'}^*}\right] + \frac{i\Gamma_n}{\pi}\frac{\zeta_n}{(\zeta_n^2 - 1)^2} \tag{6}$$

The mathematical form of the Kelvin theorem is

$$\frac{\mathrm{d}z_n}{\mathrm{d}t} = w(z_n) \tag{7}$$

$$\Gamma_n = \text{const} \tag{8}$$

Equation (7) is numerically integrated by means of the second-order Adams–Bashforth scheme as follows:

$$z_n|_{t+\Delta t} = z_n|_t + \frac{1}{2}(3w_n|_t - w_n|_{t-\Delta t})\Delta t \tag{9}$$

It is clear from the above derivation that, once Γ_n and ζ_n are given at the initial time t_0, the motion of the vortices, and thus the distribution of the circulation in the flowfield, can be determined at subsequent times.

It is a major step of the present method to model the vortex shedding at the edges of the slit. To do this, the method proposed by Brown and Michael [16] is employed, in which the shed vortices are represented by a concentrated point vortex that is connected to the slit edge by a vortex-free feeding sheet, as sketched in Fig. 3. The details of Brown and Michael's vortex-shedding model is presented in the Appendix. At each time step, the strength and location and of the nascent vortices from the slit edges are determined by Eqs. (A2) and (A13), respectively.

B. Quasi-Three-Dimensional Strategy for the Computation of the Far-Field Unsteady Pressure Difference

As shown in Fig. 4, the Bernoulli equation is applied along path ACB to obtain the far-field pressure difference across the slit plate, as written below:

$$p_A - p_B = -\frac{\mathrm{d}\Gamma_{t,l}}{\mathrm{d}t} + \frac{\partial}{\partial t}\int_A^B \mathbf{u}_\Gamma\cdot\mathrm{d}\boldsymbol{l} + \frac{\partial}{\partial t}\int_A^B \mathbf{u}_Q\cdot\mathrm{d}\boldsymbol{l} \tag{10}$$

The condition that $|\mathbf{u}_A| \to 0$ and $|\mathbf{u}_B| \to 0$ as $A \to +\infty$ and $B \to -\infty$ has been used in deriving the above equation. However, a tricky problem immediately emerges in that the path integral of the last term in the right side of Eq. (10) becomes divergent as the end points, A and B, go into the far field, extending to infinity, if the flow is assumed to be 2-D everywhere. A similar problem has been encountered in the previous studies of the nonlinear acoustics of the pipe exit. Disselhorst and Van Wijngaarden [17] proposed that the pressure difference be obtained by subtracting from the above equation the result that would occur if no vortices were present. In this way, although the divergent term in the Bernoulli equation is canceled out, the pressure difference thus obtained is only associated with the acoustic resistance of the slit due to the presence of the vortices. Thus, it is still a problem to compute the acoustic reactance of the slit that is related to the unsteady potential flow in the neighborhood of the slit. Here, we recognize that the unphysical divergence of the far-field pressure difference results from the fact that, in reality, a complete 2-D flow does not exist in an open domain extending to infinity. As the observer point moves far away from the slit, the 3-D effect must be taken into account, even if the aspect ratio is very large. Therefore, we propose a quasi-3-D strategy to deal with the problem raised in the above discussion. The basic idea is that the far-field difference of the velocity potential due to the fluctuating flow through the slit is given by a quasi-3-D potential function Φ_Q instead of the complete 2-D one W_Q. By means of the half-space Green's function of the Laplace equation for the incompressible potential flow, we can write

$$\Phi_Q(x_1, x_2, x_3) = \Phi_{Q,\pm\infty} \mp \frac{1}{2\pi}\int_{-b/2}^{b/2}\int_{-1}^{1}\frac{\partial\Phi_Q}{\partial x_2'}\frac{\mathrm{d}x_1'\mathrm{d}x_3'}{\sqrt{(x_1 - x_1')^2 + (x_3 - x_3')^2 + x_2^2}} \tag{11}$$

Then, because Φ_Q and $\partial\Phi_Q/\partial x_2$ are continuous across the slit, we derive from the above equation that

$$\int_{-\infty}^{+\infty}\mathbf{u}_Q\cdot\mathrm{d}\boldsymbol{l} = \Phi_{Q,+\infty} - \Phi_{Q,-\infty} = \frac{1}{\pi}\int_{-b/2}^{b/2}\int_{-1}^{1}\frac{\partial\Phi_Q}{\partial x_2'}\frac{\mathrm{d}x_1'\mathrm{d}x_3'}{\sqrt{(x_1 - x_1')^2 + (x_3 - x_3')^2}} \tag{12}$$

Based on the assumption of quasi-3-D flow, Φ_Q can be well approximated by W_Q in the vicinity of the slit. Thus,

$$\frac{\partial\Phi}{\partial x_2} \cong \frac{\mathrm{d}W_Q}{\mathrm{d}z} = \frac{Q(t)}{\pi}\frac{1}{\sqrt{1 - x_1^2}} \tag{13}$$

Substituting the above equation into Eq. (12), and performing a spanwise averaging in the way that both sides of the equation are integrated over $-b/2 \le x_3 \le b/2$, we obtain

$$\int_{-\infty}^{+\infty}\mathbf{u}_Q\cdot\mathrm{d}\boldsymbol{l} = \frac{Q(t)}{\pi^2 b}\int_{-1}^{1}\frac{F(x_1, x_1')}{\sqrt{1 - x_1'^2}}\,\mathrm{d}x_1' \tag{14}$$

where

$$F(x, x') = \int_{-b/2}^{b/2}\int_{-b/2}^{b/2}\frac{\mathrm{d}x_3'\mathrm{d}x_3}{\sqrt{(x_1 - x_1')^2 + (x_3 - x_3')^2}} = -2b\{\ell_n|x_1 - x_1'| - \ell_n[b + \sqrt{b^2 + (x_1 - x_1')^2}] + \sqrt{1 + (x_1 - x_1')^2/b^2} - |x_1 - x_1'|/b\}$$

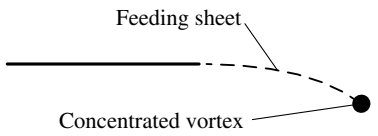

Fig. 3 Schematic of the Brown and Michael model of vortex shedding from the edge of a thin plate [16].

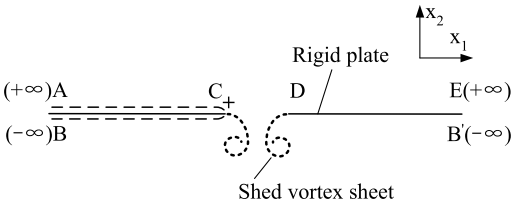

Fig. 4 Path ACB along which the Bernoulli equation is applied.

Then, we define a spanwise-averaged inertia coefficient C so that Eq. (14) can be rewritten as

$$\int_{-\infty}^{+\infty} \mathbf{u}_Q \cdot \mathrm{d}\boldsymbol{l} = Q(t)C \tag{15}$$

As shown in Fig. 5, C is a function of the aspect ratio or the normalized b, i.e., $C = C(b)$. By means of this strategy, the path integral

$$\int_{-\infty}^{+\infty} \mathbf{u}_Q \cdot \mathrm{d}\boldsymbol{l}$$

makes a finite contribution to the pressure difference across the slit.

The path integral of $\vec{u}_\Gamma$ in Eq. (10) has no problem with convergency, and it is straightforwardly written as

$$\int_A^B \mathbf{u}_\Gamma \cdot \mathrm{d}\boldsymbol{l} = \sum_{n=1}^{N} \frac{\Gamma_n}{\pi}\left[\frac{\pi}{2} - \arctan\left(\frac{\xi_{1n}}{\xi_{2n}}\right)\right] \tag{16}$$

Then, substituting Eqs. (15) and (16) into Eq. (10), we arrive at

$$p_i = p_A - p_B = -\frac{\mathrm{d}\Gamma_t}{\mathrm{d}t} + \frac{\partial}{\partial t}\left[\sum_{n=1}^{N} \frac{\Gamma_n}{\pi}\left(\frac{\pi}{2} - \arctan\frac{\xi_{1n}}{\xi_{2n}}\right)\right] + C(b)\frac{\partial Q(t)}{\partial t} \tag{17}$$

C. Computation of Unsteady Flow

The unsteady vortical and velocity flowfields of the slit under the sinusoidal pressure excitation, $p_i = P\cos\omega t$, is computed in the time domain. A typical time step of the time-marching approach is performed as follows:

1) Evaluate $Q(t)$ from Eq. (17). The rate of the vortex circulation shed from the left slit edge is given by

$$\frac{\mathrm{d}\Gamma_t}{\mathrm{d}t} = \frac{\Gamma_1}{\mathrm{d}t} \tag{18}$$

Note that the time marching begins at the initial time t_0 of a small value, and the initial condition is approximately $\Gamma_1(t_0) = 0$.

2) Calculate the coordinates of the nascent vortices according to Eq. (A13), and then update the positions of all the point vortices from solving Eq. (6) by means of the Adams–Bashforth integration scheme [Eq. (9)].

3) Release the two nascent vortices by assigning them the circulations given by the Kutta condition, and introduce a small cutoff radius for the nascent vortices as an artificial smoothing parameter. A smoothing technique is very helpful in preventing the excessive instability of the discrete vortex system, thus obtaining the reasonably clean and organized flow pattern. In the present simulation, the well-used method is employed that treats each point vortex as a vortex blob with a cutoff radius to avoid the unbounded velocity near the point vortex [18]. Assuming the vortex blob is of a Rankine type, the induced velocity of a point vortex with a cutoff radius is given by the following equation:

$$w^* = \frac{\Gamma_{n'}}{2\pi i}\frac{1}{\zeta_n - \zeta_{n'}}\begin{cases} 1 & (|\zeta_n - \zeta_{n'}| > r_c) \\ r_c^{-2}|\zeta_n - \zeta_{n'}|^2 & (|\zeta_n - \zeta_{n'}| \le r_c) \end{cases} \tag{19}$$

where the cutoff radius $r_c = \kappa d$, in which κ is a selected constant smaller than unity. In the present simulation, κ varies within the range from 0.8 to 0.9. According to the numerical tests, the simulation results are not sensitive to the exact choice of κ.

4) Shift the indices of the vortices as follows:

$$\Gamma_{n+2,\mathrm{new}} = \Gamma_{n,\mathrm{previous}}, \zeta_{n+2,\mathrm{new}} = \zeta_{n,\mathrm{previous}}, w_{n+2,\mathrm{new}} = w_{n,\mathrm{previous}} \tag{20}$$

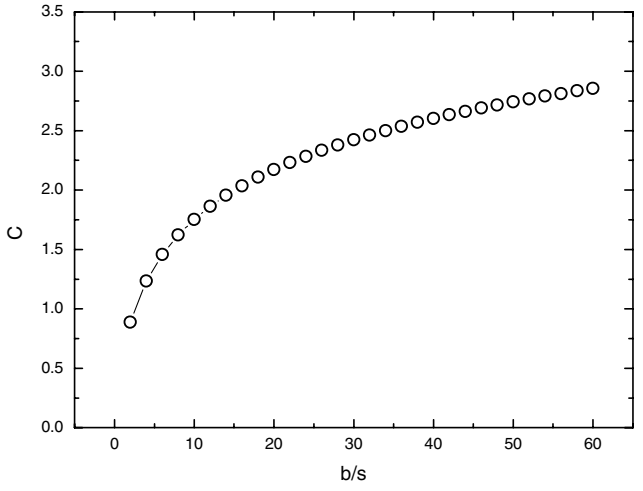

Fig. 5 Inertia coefficient C as a function of aspect ratio of the slit.

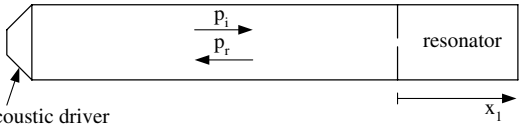

Fig. 6 Impedance tube with a slit resonator at the right end.

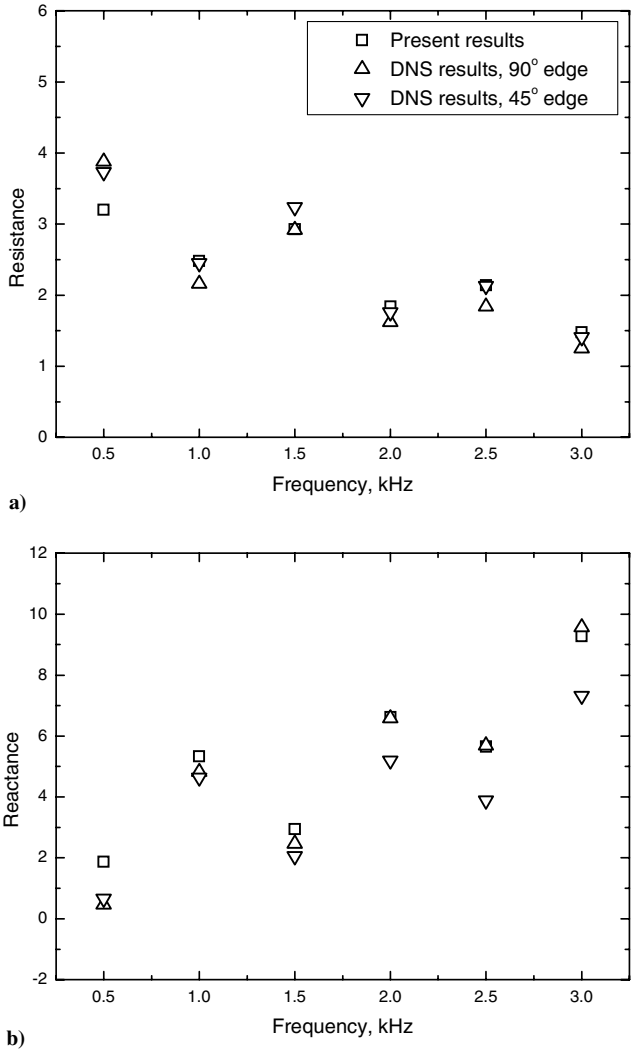

Fig. 7 Comparison between present results and DNS results in [13] for the normalized specific acoustic impedance of the resonator with a 0.05-in.-wide slit: a) acoustic resistance and b) acoustic reactance.

5) Increment the time by the interval

$$t_m = t_{m-1} + \Delta t \tag{21}$$

To limit the computation time, each vortex is gradually damped; that is, its circulation is decreased as it is convected away from the slit, so it is eventually not involved in the computation when its circulation becomes zero.

D. Computation of the Acoustic Impedance

Strictly speaking, the definition of acoustic impedance refers to the relation between the acoustic pressure and the acoustic particle velocity in which both are sinusoidal in time. However, due to the occurrence of the nonlinear distortion, the average velocity through the slit v_{av} is periodic but deviates somewhat from being sinusoidal. So, Fourier decomposition is employed to get the spectrum of the average velocity as a function of time. Provided that the first harmonic component is dominant in the spectrum of the average velocity, the nonlinear acoustic impedance of the slit can be defined as below, according to Ingard and Ising [9]:

$$r = ks\frac{P\cos[\phi(1)]}{v_{\text{av}}(1)}, \qquad x = -ks\frac{P\sin[\phi(1)]}{v_{\text{av}}(1)} \tag{22}$$

The acoustic impedance is normalized by ρc throughout this paper.

III. Results and Discussion

A. Comparison with Direct Numerical Simulation Results

In [13], a DNS method is used to simulate the acoustic experiment carried out on a slit resonator in the normal incidence tube at NASA Langley Research Center. The experimental setup is as illustrated in Fig. 6. The slit resonator consists of a single slit centered in a 2 in.^{2}, 0.04-in-thick facesheet covering a 6-in.-deep cavity of the same cross section. Slits of three different sizes are tested. Their 2 in. lengths just span the dimension of the impedance tube, and their widths are 0.05, 0.1, and 0.2 in. The acoustic problem of the slit resonator can be separated into three different physical processes: 1) the sound propagation in the impedance tube, 2) the local absorption at the slit due to a finite pressure difference between the tube and the back cavity, and 3) the enhancement of the absorption due to resonance. Here, the first and the third physical processes are treated by the one-dimensional (1-D) sound propagation model. The second physical process is solved by the present DVM neglecting the influence of the walls of the tube and the cavity. The effects of the facesheet thickness and the angle of the slit edge are also neglected.

From the model of 1-D sound propagation inside the cavity, we can obtain the sound pressure on the right side of the facesheet, $x_1 = 0^+$:

$$p_{x_1=0^+} = -i\rho c u^+ \cot\left(\frac{\omega D}{c}\right) \tag{23}$$

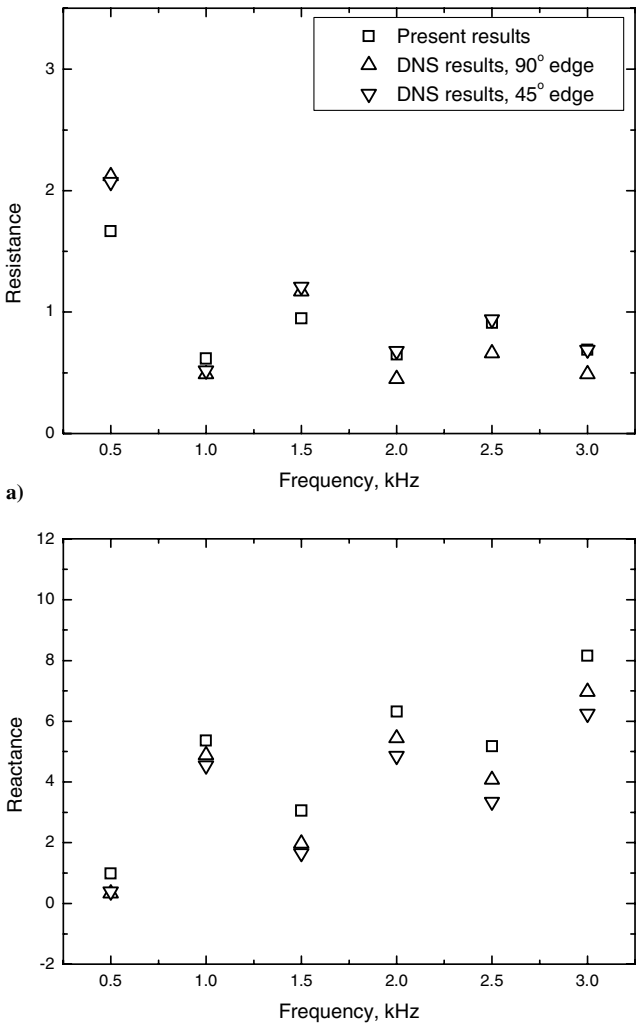

Fig. 8 Comparison between present results and DNS results in [13] for the normalized specific acoustic impedance of a resonator with a 0.1-in.-wide slit: a) acoustic resistance and b) acoustic reactance.

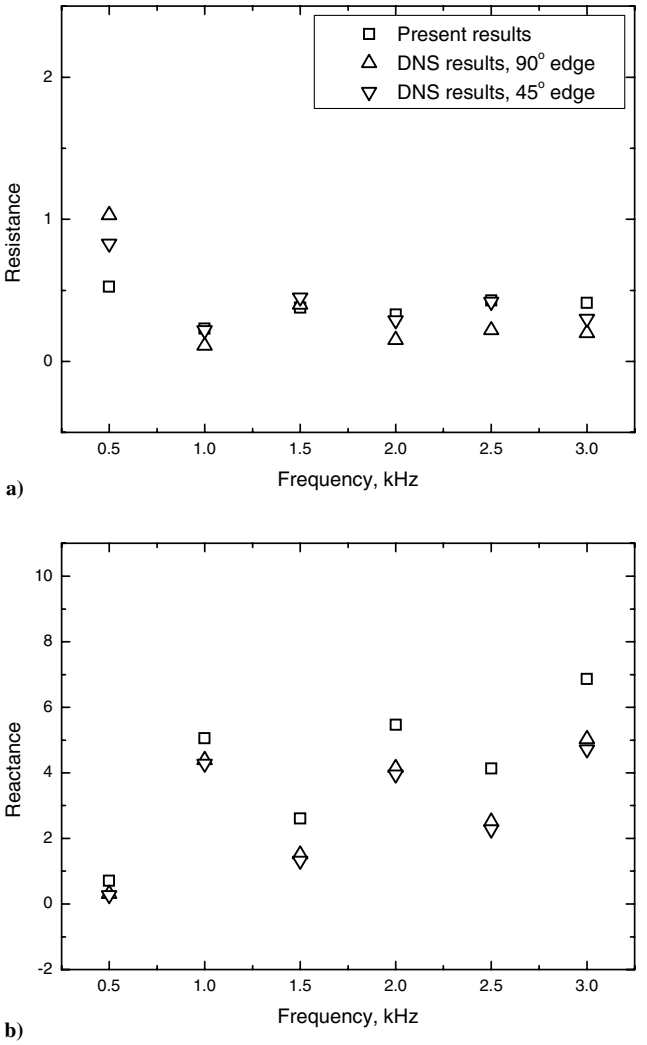

Fig. 9 Comparison between present results and DNS results in [13] for the normalized specific acoustic impedance of the resonator with a 0.2-in.-wide slit: a) acoustic resistance and b) acoustic reactance.

Table 1 Geometrical parameters of the slits

Number	Half-width s, mm	Aspect ratio AR
1	1.585	5
2	1.121	10
3	0.915	15

Thus, we can obtain the acoustic impedance of the resonator cavity as

$$Z_{\text{cavity}} = -i\cot\left(\frac{\omega D}{c}\right) \tag{24}$$

The mathematical definition of the acoustic impedance of the slit is as follows:

$$Z_{\text{slit}} = \frac{p_{x_1=0^-} - p_{x_1=0^+}}{\rho c v_{\text{ac}}} \tag{25}$$

In the local region around the slit, the following mass continuity relation holds:

$$u^{\pm} = \sigma v_{\text{ac}} \tag{26}$$

The combination of Eqs. (23–26) leads to the acoustic impedance of the slit resonator Z_{res}:

$$Z_{\text{res}} = \frac{Z_{\text{slit}}}{\sigma} - i\cot\left(\frac{\omega D}{c}\right) \tag{27}$$

From the 1-D model for the sound propagation in the impedance tube, the total sound pressure on the left side of the facesheet, $x_1 = 0^-$, can be related to the incident sound wave from the sound source; that is,

$$p_{x_1=0^-} = \frac{2Z_{\text{res}}}{Z_{\text{res}} + 1} p_i \tag{28}$$

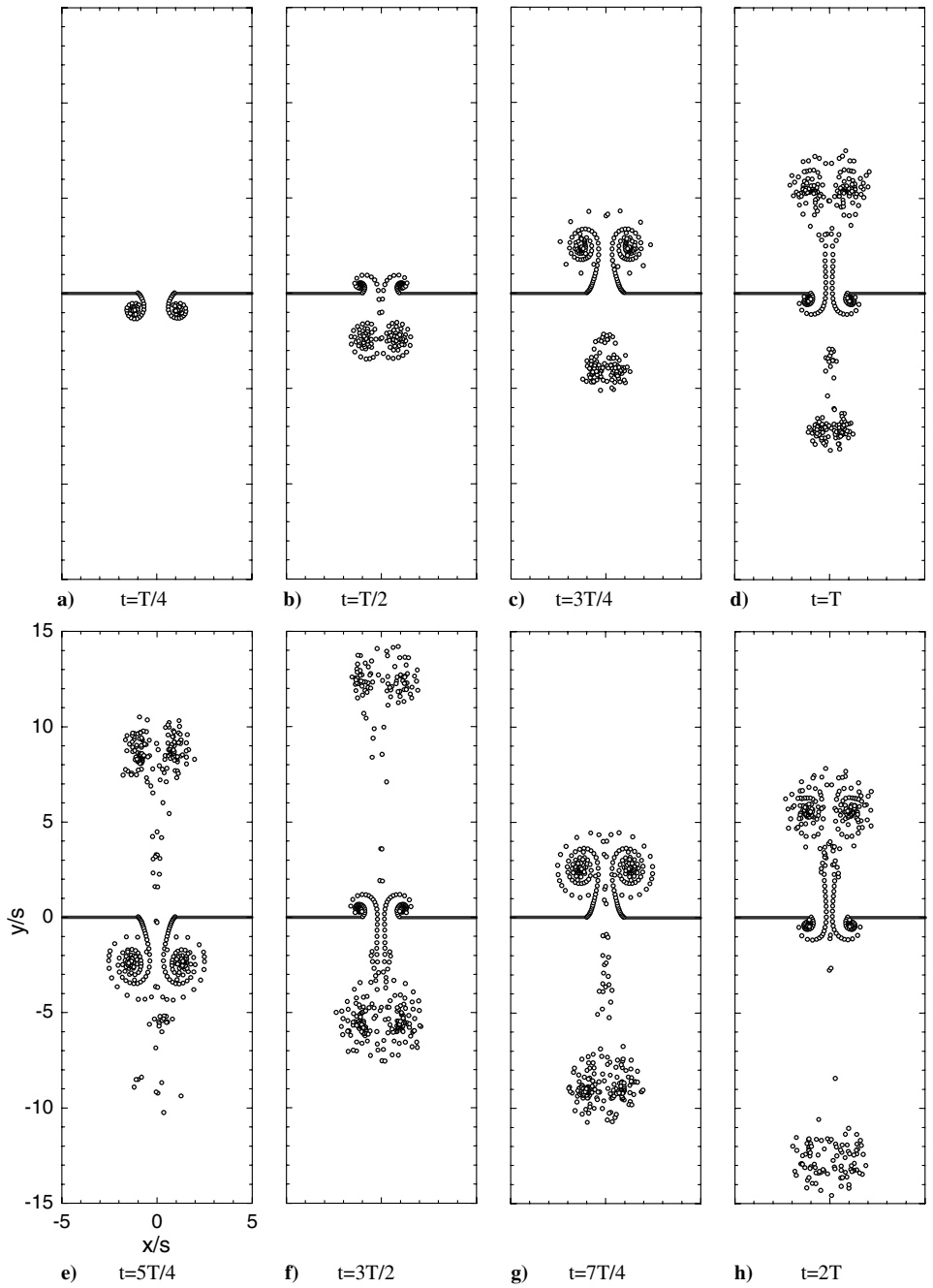

Fig. 10 Vortex-shedding process and the evolution of the vortices at a slit subjected to high-intensity sound.

Thus, the pressure difference between the two sides of the facesheet can be derived from Eqs. (23), (26), and (28):

$$\Delta p_{x_1=0} = p_{x_1=0^-} - p_{x_1=0^+} = \frac{2Z_{\text{res}}}{Z_{\text{res}}+1} p_i + i\rho c\sigma \cot\left(\frac{\omega D}{c}\right) v_{\text{av}} \tag{29}$$

The calculation of the acoustic impedance of the resonator is done in the following steps:

1) Input $\Delta p_{x_1=0}$ into the DVM as the sound pressure difference across the orifice plate to obtain the values of v_{av}, Z_{slit}, and then Z_{res} from Eq. (27).

2) Substitute v_{av} and Z_{res} into Eq. (29) to calculate $\Delta p_{x_1=0}$.

3) Repeat steps 1–2 until Z_{res} converges.

When the above iteration is initialized, the incident sound pressure p_i is used to approximate $\Delta p_{x_1=0}$.

The present and Tam et al.'s [13,14] DNS results for the acoustic impedance of the slit resonators are compared at six frequencies near the resonance and antiresonance of the resonators, as presented in Figs. 7–9. But as mentioned, the conditions of the two models are not completely identical. One difference of the present model with the DNS is that the plate thickness is not considered. As we can see, for the three sizes of slits with a 45° edge, the present results for acoustic resistance agree well with the DNS results, except for the frequency of 500 Hz where the acoustic resistance markedly increases due to resonance. This is well expected since the effect of plate thickness can be largely removed by sharpening the edge of the slit, as is usually done in experiments to approximate to the thin-plate condition. For the slits with a 90° edge, however, the plate thickness must take its effect in some manner. Therefore, it is also understandable that the present results for acoustic resistance have some differences with the DNS results. When comparing the acoustic reactance obtained by the two methods, the two results are consistent in their trend but deviate somewhat from each other in their values. In fact, it is not rare that the data of acoustic reactance are more scattered than acoustic resistance in the measurement or numerical simulation of the orifice acoustic properties, especially when the flow at the orifice is under the influence of shedding vortices. Generally speaking, the present DVM provides very similar trends and reasonably good agreement in values with the computationally intensive DNS model. Note that the present model does not include the viscous effect. So, this agreement suggests that the acoustic damping due to the viscous effect is not dominant, such that the acoustic absorption due to the sound–vortex interaction is increasingly important for high sound intensity.

B. Acoustic Nonlinearity of a Slit

1. *Flow Pattern of the Shedding Vortices*

In this section and hereafter, the nondimensionalized sound pressure and acoustic particle velocity are converted to the dimensional values in the units of pascals (or decibels) and meters per second, respectively, in order to easily evaluate their real magnitudes or compare the present results with the data of other sources if needed.

It has long been noticed that the unsteady vortices are shed when high-intensity sound impinges upon the rim of an orifice. This vortex-shedding mechanism is important because it accounts for the nonlinear acoustic impedance of the orifice. It is assumed that the fluctuating flow of the slit is dominated by the vortex shedding occurring at the long edges of the slit with a large aspect ratio.

The present computation is carried out for three slits, i.e., numbers 1–3 slits with parameters given in Table 1. In Fig. 10, for the number 2 slit with $AR = 10$, and on the condition that $P = 300$ Pa

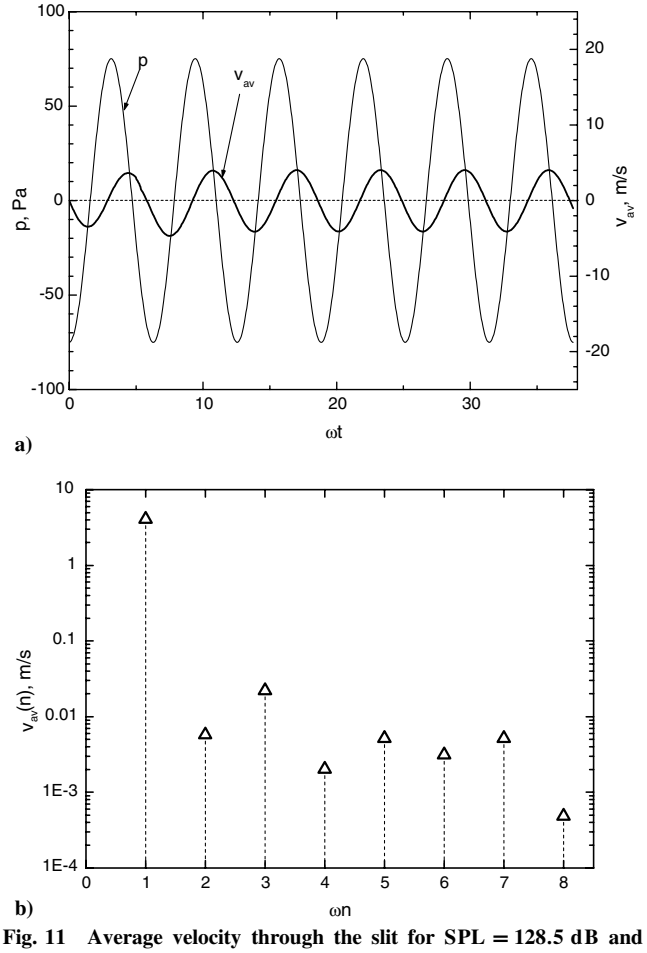

Fig. 11 Average velocity through the slit for SPL = 128.5 dB and $f = 500$ Hz: a) time history and b) spectrum.

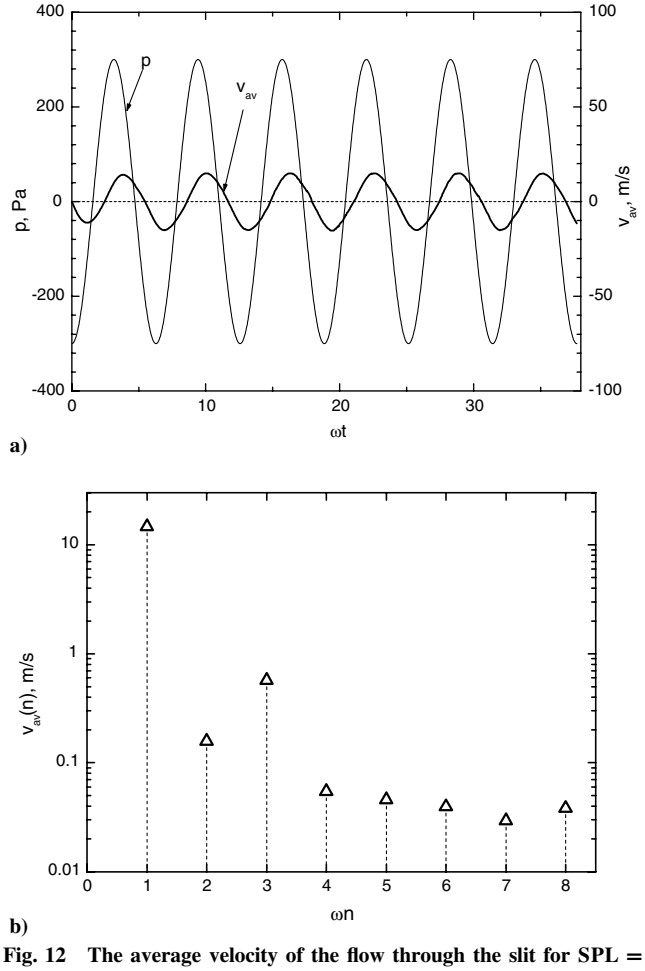

Fig. 12 The average velocity of the flow through the slit for SPL = 140.5 dB and $f = 500$ Hz : a) time history and b) spectrum.

and $f = 500$ Hz, the shedding and evolution processes of the vortices are displayed at each successive time interval of $T/4$ during the first two periods of time. The nondimensionalized time step is set to be 0.005 in the simulation.

As depicted by the numerical simulation, the vortices shed from the slit edges roll into a pair of spiral-like counter-rotating vortices at the beginning of the time period. As it grows larger and larger, the two vortices approach each other while moving away from the slit. At the instant of $T/2$, it can be seen that the perturbation flow through the orifice has already changed its direction, but the vortex pair moves further away from the slit, mainly due to its self-induced velocity. The regular spiral-shaped vortex is finally broken when the two vortices collide, thus forming a vortex cluster mixed with vortices rotating in the opposite directions. The above vortex evolution process is completed within one of the time period. Also, the same process is repeated at the other side of the slit lagging by half of the time period. From the qualitative point of view, the simulation of the formation, evolution, and interaction of the vortex pair at the slit shows marked resemblance with the previous particle image velocimetry (PIV) flow visualization [19].

2. *Time History of the Acoustic-Driven Slit Flow*

The average velocity of the acoustic-driven flow through the slit v_{av} is of concern because of its importance in calculating the acoustic impedance of the slit, as defined by Eq. (22). When the frequency is 500 Hz, the time history of v_{av} is computed for the number 2 slit at three sound pressure levels (SPLs) (128.5, 140.5, and 148.5 dB), and the results are presented in Figs. 11a, 12a, and 13a, respectively. As we can see, the curve of v_{av} repeats itself for each period after only the first one. Thus, the rapid convergence of the computation is demonstrated. The time-history curve of v_{av} is nearly sinusoidal at a relatively low SPL of 128.5 dB, whereas it exhibits obvious nonlinear distortion when the SPL is increased to 148.5 dB. The Fourier spectrums of v_{av} are given in Figs. 11b, 12b, and 13b correspondingly for the three SPLs. We can see that the higher-order harmonic components appear in the spectrum of v_{av}, and their amplitudes increase with the increase of SPL. However, even at high SPLs, the fundamental harmonic component still plays a dominant role with its amplitude being 10 times larger than those of the higher-order harmonic components.

In Fig. 14, the amplitude and phase of the fundamental harmonic component of the average velocity of the slit flow, $v_{\text{av}}(1)$ and $\phi(1)$, respectively, are plotted as a function of the SPL. The results for the three slits with different aspect ratios are presented for comparison in the figure. Note that the area of the slits is kept constant, with the value being 12.56 mm^2. The figure shows that, as SPL increases, $v_{\text{av}}(1)$ increases while $\phi(1)$ decreases in its absolute value, showing that v_{av} is gradually in phase with the driving sound pressure. It is also shown that, for the parametric range in this study, $v_{\text{av}}(1)$ increases while the absolute value of $\phi(1)$ decreases to some extent as the aspect ratio increases. However, when the SPL is very high (exceeding 145 dB in the present case), the influence of AR gradually diminishes.

3. *Nonlinear Acoustic Impedance*

The nonlinear acoustic impedance is calculated according to Eq. (22), and the results for the three slits in Table 1 are presented in Fig. 15. It is shown that the acoustic resistance increases markedly with the SPL, whereas the acoustic reactance decreases to some extent. As the aspect ratio is increased from 5 to 15, the nonlinear

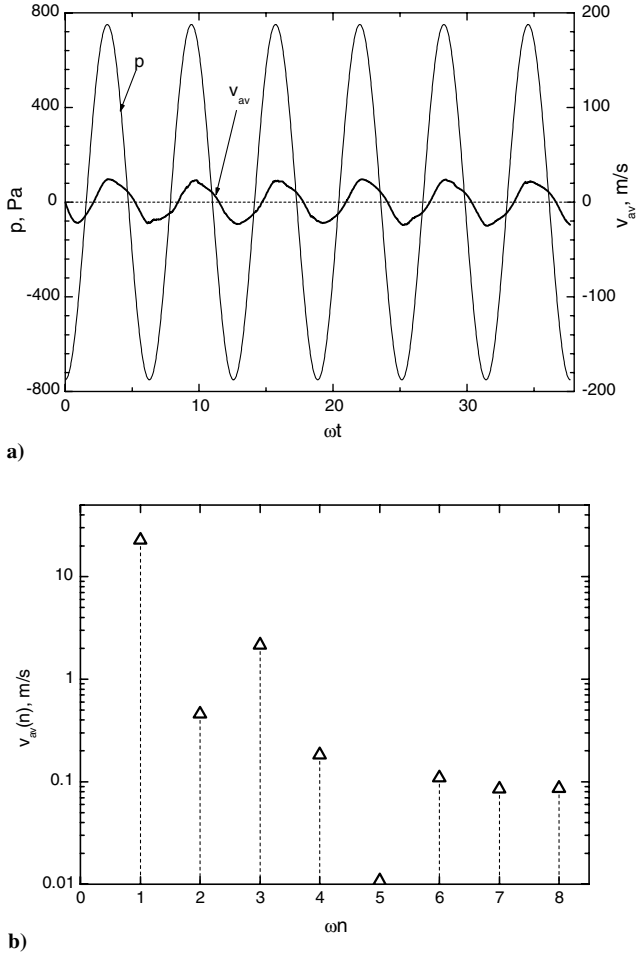

Fig. 13 Average velocity of the flow through the slit for SPL = 148.5 dB and $f = 500$ Hz: a) time history and b) spectrum.

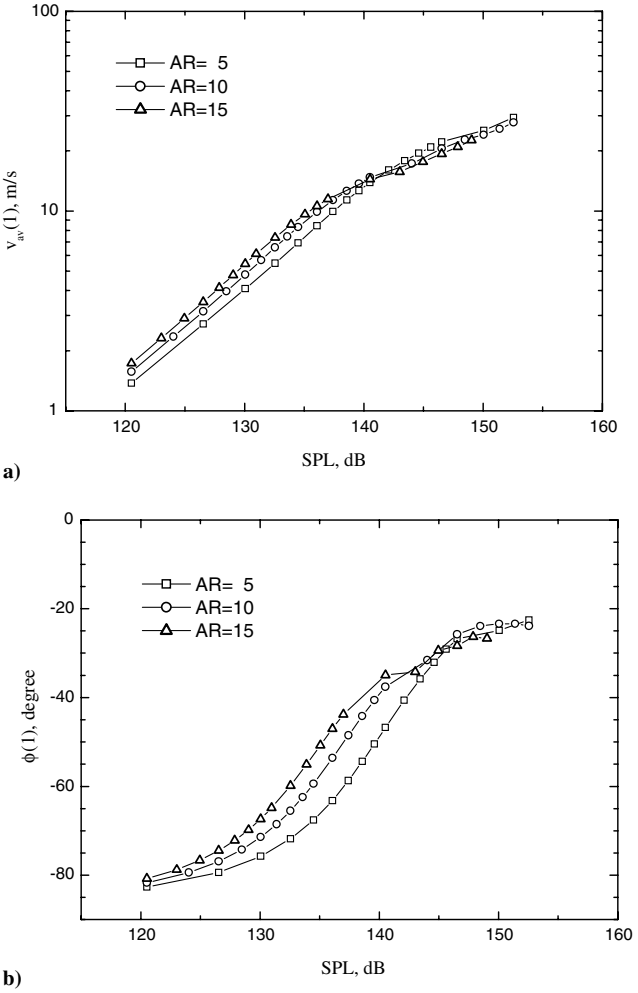

Fig. 14 Magnitude and phase of the fundamental harmonic of the average velocity through the slit as a function of the applied SPL for different aspect ratios: a) magnitude and b) phase.

acoustic resistance slightly increases, whereas the nonlinear acoustic reactance decreases. Obviously the acoustic reactance changes with AR more prominently than the acoustic resistance. The nonlinear acoustic impedance of a circular orifice, computed by the method of [15], is also presented in Fig. 15 for comparison. The circular orifice has an equivalent radius of 4.0 mm by the requirement of its area being equal to that of the slits. From the figure, we can see that, as AR increases, the acoustic resistance and reactance of the slits show slightly increasing and obviously decreasing trends, respectively, compared with those of the circular orifice. Similar to the above analysis regarding the average velocity, the influence of the aspect ratio or the orifice shape on acoustic impedance tends to be less important when the SPL exceeds a certain high value (around 145 dB in the present case).

4. Discharge Coefficient

As shown in Fig. 10, the vortex evolution leads to the formation of a slit jet for which the cross section gradually contracts and reaches its minimum at the so-called vena contracta. Because of this phenomenon, the average velocity through the slit is smaller than the jet velocity at the the vena contracta. The discharge coefficient is defined as the ratio of the average velocity to the vena contracta velocity:

$$C_D = \frac{v_{\text{av}}}{v_{\text{VC}}} \cong \frac{\bar{v}_{\text{av}}(1)}{\sqrt{2\bar{P}}} \tag{30}$$

In Fig. 16, C_D is plotted as a function of the SPL for three aspect ratios. It is shown that Cd increases with AR at relatively low SPL,

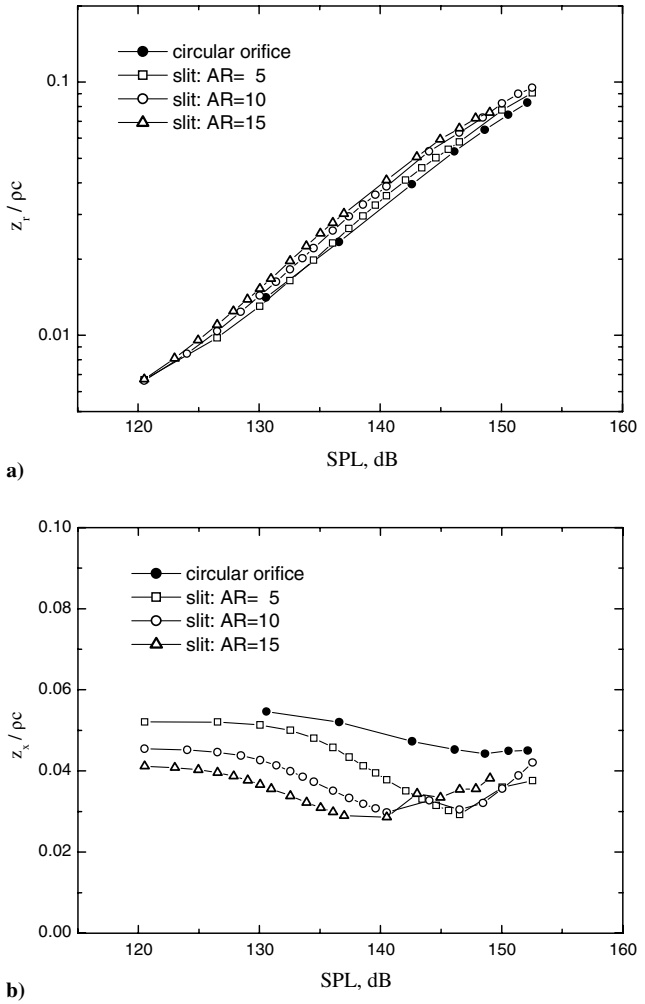

Fig. 15 Normalized specific acoustic impedance as a function of the applied SPL for different aspect ratios or orifice shape: a) acoustic resistance and b) acoustic reactance.

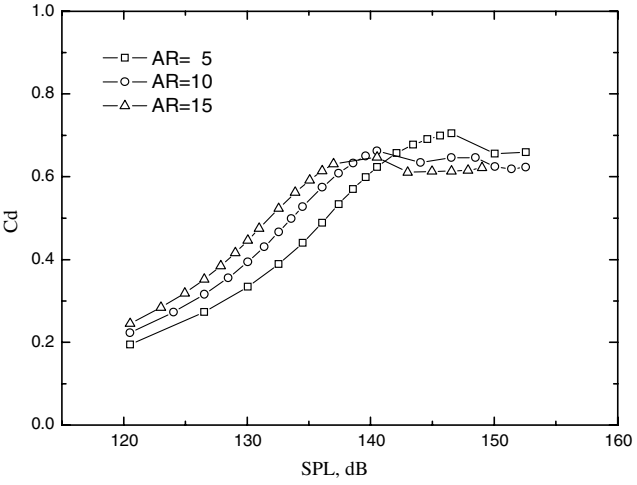

Fig. 16 Discharge coefficient as a function of the applied SPL for different aspect ratios.

whereas the tendency is reversed at high SPL. The influence of the SPL on C_D is far more prominent than AR. Generally, C_D increases with the increase of SPL and asymptotically approaches a value of about 0.62–0.64. This asymptotic value given by the present unsteady flow model agrees well with Rouse's result [20] and is well within the range of 0.61–0.64 given by Batchelor [21]. Both Rouse's [20] and Batchelor's [21] results are obtained from the static flow models. The discharge coefficient is important because it is a crucial factor in establishing the quasi-steady impedance models of small orifices for engineering application purposes. However, in most quasi-steady impedance models, the discharge coefficient is introduced by the empirical means of fitting the model with the experimental data. In the present model, the discharge coefficient of a slit is a direct result from the fully unsteady flow model that includes the effect of vortex shedding.

IV. Conclusions

In this paper, the sound-excited nonlinear vortex shedding at a slit orifice and its acoustic effect are studied by means of quasi-3-D DVM. The present approach employs the conventional DVM to simulate the 2-D unsteady vortical flow around the slit and uses a spanwise-averaged 3-D Green's function to connect the near-field flow quantities with the far-field fluctuating pressure difference. As a result, the problem of logarithmic divergence in the dynamical equilibrium relation specific to the 2-D orifice or sink flow is solved. The main findings of the present study are summarized as follows:

1) The generally good agreement between the present inviscid model and the viscous DNS model suggests that the acoustic damping due to the viscous effect is not dominant, such that the acoustic absorption due to the sound–vortex interaction is increasingly important for high sound intensity.

2) The simulated flow pattern of the shedding vortices at the slit is consistent with the previous PIV flow visualization, showing the feature that the oscillatory slit flow is dominated by a pair of spiral-like counter-rotating vortices moving away from the slit and eventually colliding into each other.

3) Because of the vortex shedding, nonlinear distortion occurs in the average velocity of the oscillatory slit flow under sinusoidal sound excitation. However, the fundamental harmonic of the average velocity plays such a dominant role that its amplitude is 10 times larger than those of the higher harmonics.

4) The nonlinear acoustic resistance of the slit orifice correspondingly increases, whereas the nonlinear acoustic reactance decreases to some extent with increasing amplitude of the applied sound pressure.

5) For the parametric range in this study, as the aspect ratio increases while keeping the orifice area constant, the acoustic resistance and reactance of the slits show slightly increasing and

obviously decreasing trends, respectively, compared with those of the circular orifice. However, the influence of the aspect ratio or the orifice shape on acoustic impedance tends to be less important when the SPL exceeds a certain high value.

6) The discharge coefficient of the slit, defined by the ratio between the average velocity through the slit and the maximum velocity at the vena contracta, increases with increasing SPL and asymptotically approaches a value within the range of 0.62–0.64 that is consistent with the steady flow analysis.

Appendix : Brown and Michael Vortex-Shedding Model

The circulation of the nascent vortices is determined by the application of the Kutta condition, requiring the velocity of inviscid flow to be finite at a boundary discontinuity like the slit edges. Thus, Γ_1 satisfies the following relation at the left edge of the slit or $\zeta = -1$ where the transformation $\mathrm{d}\zeta/\mathrm{d}z$ is singular:

$$\lim_{\zeta\to-1}\frac{\mathrm{d}}{\mathrm{d}\zeta}\left[W(\zeta)+\frac{\Gamma_1}{2\pi i}\ell_n\frac{\zeta-\zeta_1}{\zeta-\zeta_1^*}\right]=0 \tag{A1}$$

This gives

$$\Gamma_1 = 2\pi i W'(-1)\frac{(1+\zeta_1)(1+\zeta_1^*)}{\zeta_1^*-\zeta_1} \tag{A2}$$

The above equation indicates that Γ_1 is a function of the position as the nascent vortex is convected away from the edge. Thus, an unsteady force is induced and acts on the feed sheet that must be compensated by a counterforce acting on the nascent vortex, since the point vortex-feed sheet combination, representing the original vortex sheet released from the slit edge, cannot sustain a net force action. This leads to the following equation for the circulation and the position of the nascent point vortex, as proposed by Rott [22]:

$$\frac{\mathrm{d}z_1}{\mathrm{d}t}+\frac{z_1-z_e}{\Gamma_1}\frac{\mathrm{d}\Gamma_1}{\mathrm{d}t}=w(z_1) \tag{A3}$$

Because the motion of nascent point vortex is within a region very close to the slit edge, the conformal mapping equation (2) can be simplified as

$$z_1+1=-\frac{1}{2}(\zeta_1+1)^2 \tag{A4}$$

Using Eq. (A4), Eq. (A3) can be rewritten as follows:

$$-(\zeta_1+1)\frac{\mathrm{d}\zeta_1}{\mathrm{d}t}-\frac{1}{2}(\zeta_1+1)^2\frac{1}{\Gamma_1}\frac{\mathrm{d}\Gamma_1}{\mathrm{d}t}=w(z_1) \tag{A5}$$

Substituting Eq. (A2) into Eq. (A5), we get

$$-(\zeta_1+1)\frac{\mathrm{d}\zeta_1}{\mathrm{d}t}-\frac{(\zeta_1+1)^2}{2(\zeta_1^*-\zeta_1)}\left(\frac{\zeta_1^*+1}{\zeta_1+1}\frac{\mathrm{d}\zeta_1}{\mathrm{d}t}-\frac{\zeta_1+1}{\zeta_1^*+1}\frac{\mathrm{d}\zeta_1^*}{\mathrm{d}t}\right)$$
$$-\frac{1}{2}(\zeta_1+1)^2\frac{1}{W'(-1)}\frac{\mathrm{d}W'(-1)}{\mathrm{d}t}=w(z_1) \tag{A6}$$

However, Eq. (A6) is singular in that $W'(-1)$ is zero from the application of the Kutta condition. To handle this problem, we follow Kuo and Dowling's method [23], employing a similarity solution in collaboration with the Rott's equation. It is assumed that the nascent vortex initially moves along a straight path, so its position can be given as

$$\zeta_1=\beta t^\alpha e^{i\theta}-1 \tag{A7}$$

where α, β, and θ are constants. In addition, $W'(-1)$ is presumed to be linearly related to t:

$$W'(-1)\sim\lambda t \tag{A8}$$

The substitution of Eqs. (A7) and (A8) into Eq. (A6) results in

$$-\beta^2 t^{2\alpha-1}e^{2i\theta}\left(\frac{3}{2}\alpha+\frac{1}{2}\right)=\lim_{\zeta_1\to-1}w(z_1) \tag{A9}$$

As its position approaches the slit edge, the finite velocity of the nascent vortex is

$$\lim_{\zeta_1\to-1}w(z_1)=\frac{Q}{\pi}+\sum_{n=3}^{N}\frac{\Gamma_n}{2\pi i}\left[\frac{1}{(\zeta_n+1)^2}-\frac{1}{(\zeta_n^*+1)^2}\right]$$
$$+\frac{\Gamma_1}{2\pi i}\frac{1}{\zeta_1+1}\left[-\frac{1}{2(\zeta_1+1)}+\frac{1}{\zeta_1-\zeta_1^*}+\frac{1}{\zeta_1^*+1}\right]+\mathcal{O}(\zeta_1+1) \tag{A10}$$

From Eqs. (A2) and (A8), it can be deduced that Γ_1 is proportional to $t^{\alpha+1}$. Hence, after retaining the nonzero leading term and ignoring the terms proportional to $t^{1-\alpha}$, Eq. (A10) is rewritten as

$$-\beta^2 t^{2\alpha-1}e^{2i\theta}\left(\frac{3}{2}\alpha+\frac{1}{2}\right)=\frac{Q}{\pi}+\sum_{n=3}^{N}\frac{\Gamma_n}{2\pi i}\left[\frac{1}{(\zeta_n+1)^2}-\frac{1}{(\zeta_n^*+1)^2}\right] \tag{A11}$$

Then, α can be obtained by balancing the power of t of the leading terms in Eq. (A11). We can also obtain the value of θ because the right-hand side of Eq. (A11) is real. The results are

$$\alpha=\frac{1}{2},\qquad \theta=\frac{\pi}{2}\quad\text{and}$$
$$\beta^2=\frac{4}{5}\left\{\frac{Q}{\pi}+\sum_{n=3}^{N}\frac{\Gamma_n}{2\pi i}\left[\frac{1}{(\zeta_n+1)^2}-\frac{1}{(\zeta_n^*+1)^2}\right]\right\} \tag{A12}$$

With the constants α, β, and θ being obtained, the location of the new vortex at the end of each time step is calculated from Eq. (A7):

$$\zeta_1=\sqrt{\frac{4}{5}\left\{\frac{Q}{\pi}+\sum_{n=3}^{N}\frac{\Gamma_n}{2\pi i}\left[\frac{1}{(\zeta_n+1)^2}-\frac{1}{(\zeta_n^*+1)^2}\right]\right\}\Delta t}-1 \tag{A13}$$

So, the strength of the new vortex at the left edge is determined from Eq. (A2). In the exact same way, the location and strength of the nascent vortex at the right edge can be obtained.

Acknowledgment

The financial support of the National Natural Science Foundation of China is gratefully acknowledged (grant numbers 50736007, 51076005, and 50890181).

References

[1] Smits, J. M. A., and Kosten, C. W., "Sound Absorption by Slit Resonators," *Acustica*, Vol. 1, 1951, pp. 114–122.

[2] Gomperts, M. C., "The 'Sound Insulation' of Circular and Slit-Shaped Apertures," *Acustica*, Vol. 14, No. 1, 1964, pp. 1–16.

[3] Monkewitz, P. A., "The Response of Helmholtz Resonators to External Excitation, Part 2: Arrays of Slit Resonators," *Journal of Fluid Mechanics*, Vol. 156, 1985, pp. 151–166. doi:10.1017/S0022112085002038

[4] Kristiansen, U. R., and Vigran, T. E., "On the Design of Resonant Absorbers Using a Slotted Plate," *Applied Acoustics*, Vol. 43, 1994, pp. 39–48. doi:10.1016/0003-682X(94)90039-6

[5] Howe, M. S., "The Dissipation of Sound at an Edge," *Journal of Sound and Vibration*, Vol. 70, No. 3, 1980, pp. 407–411. doi:10.1016/0022-460X(80)90308-9

[6] Dowling, A. P., and Hughes, I. J., "Sound Absorption by a Screen with a Regular Array of Slits," *Journal of Sound and Vibration*, Vol. 156, No. 3, 1992, pp. 387–405. doi:10.1016/0022-460X(92)90735-G

[7] Howe, M. S., "The Influence of Vortex Shedding on the Diffraction of Sound by a Perforated Screen," *Journal of Fluid Mechanics*, Vol. 97, 1980, pp. 641–653.

doi:10.1017/S002211208000273X
[8] Ingard, U., and Labate, S., "Acoustic Circulation Effects and the Nonlinear Impedance of Orifices," *Journal of the Acoustical Society of America*, Vol. 22, 1950, pp. 211–218. doi:10.1121/1.1906591
[9] Ingard, U., and Ising, H., "Acoustic Nonlinearity of an Orifice," *Journal of the Acoustical Society of America*, Vol. 42, No. 1, 1967, pp. 6–17. doi:10.1121/1.1910576
[10] Cummings, A., and Eversman, W., "High Amplitude Acoustic Transmission Through Duct Terminations: Theory," *Journal of Sound and Vibration*, Vol. 91, No. 4, 1983, pp. 503–518. doi:10.1016/0022-460X(83)90829-5
[11] Melling, T. H., "The Acoustic Impedance of Perforates at Medium and High Sound Pressure Levels," *Journal of Sound and Vibration*, Vol. 29, 1973, pp. 1–65. doi:10.1016/S0022-460X(73)80125-7
[12] Hersh, S., Walker, B. E., and Celano, J. W., "Acoustic Behavior of Helmholtz Resonators: Part 1. Nonlinear Model," *AIAA Journal*, Vol. 41, No. 5, 2003, pp. 795–808. doi:10.2514/2.2041
[13] Tam, C. K. W., Ju, H., Jones, M. G., Watson, W. R., and Parrott, T. L., "A Computational and Experimental Study of Slit Resonators," *Journal of Sound and Vibration*, Vol. 284, 2005, pp. 947–984. doi:10.1016/j.jsv.2004.07.013
[14] Tam, C. K. W., Ju, H., Jones, M. G., Watson, W. R., and Parrott, T. L., "A Computational and Experimental Study of Resonators in Three Dimensions," *Journal of Sound and Vibration*, Vol. 329, 2010, pp. 5164–5193. doi:10.1016/j.jsv.2010.06.005
[15] Jing, X., and Sun, X., "Discrete Vortex Simulation on the Acoustic Non-Linearity of an Orifice," *AIAA Journal*, Vol. 38, No. 9, 2000, pp. 1565–1572. doi:10.2514/2.1178
[16] Brown, C. E., and Michael, W. H., "Effect of Leading Edge Separation on the Lift of a Delta Wing," *Journal of the Aeronautical Sciences*, Vol. 21, 1954, pp. 690–706.
[17] Disselhorst, J. H. M., and Van Wijingaarden, L., "Flow in the Exit of Open Pipes During Acoustic Resonance," *Journal of Fluid Mechanics*, Vol. 99, 1980, pp. 293–319. doi:10.1017/S0022112080000626
[18] Sarpkaya, T., "Computational Methods with Vortices: The 1988 Freeman Scholar Lecture," *Journal of Fluids Engineering*, Vol. 111, 1989, pp. 5–52. doi:10.1115/1.3243601
[19] Ahuja, K. K., Gaeta, R. J., Jr., and D'Agostino, M., "High Amplitude Acoustic Behavior of a Slit-Orifice Backed by a Cavity," NASA CR 2000-210635, 2000.
[20] Rouse, H., *Fluid Mechanics for Hydraulic Engineers*, McGraw–Hill, New York, 1938, p. 260.
[21] Batchelor, G. K., *An Introduction to Fluid Dynamics*, Cambridge Univ. Press, Cambridge, England, U.K., 1967, p. 388.
[22] Rott, N., "Diffraction of a Weak Shock with Vortex Generation," *Journal of Fluid Mechanics*, Vol. 1, 1956, pp. 111–128. doi:10.1017/S0022112056000081
[23] Kuo, C. Y., and Dowling, A. P., "Acoustics of a Two-Dimensional Compact Jet Impinging Normally on to a Flat Plate," *Journal of Fluid Mechanics*, Vol. 414, 2000, pp. 251–284. doi:10.1017/S0022112000008557

A. Lyrintzis
Associate Editor